Coherence properties of high-gain twin beams

A. Allevi,[1,*] O. Jedrkiewicz,[2] E. Brambilla,[1] A. Gatti,[2] J. Peřina, Jr.,[3] O. Haderka,[3] and M. Bondani[2]

[1]*Dipartimento di Scienza e Alta Tecnologia, Università degli Studi dell'Insubria and CNISM UdR Como, Via Valleggio 11, I-22100 Como, Italy*

[2]*Istituto di Fotonica e Nanotecnologie, Consiglio Nazionale delle Ricerche and CNISM UdR Como, Via Valleggio 11, I-22100 Como, Italy*

[3]*RCPTM, Joint Laboratory of Optics of Palacký University and Institute of Physics of Academy of Sciences of the Czech Republic, Faculty of Science, Palacký University, 17. listopadu 12, 77146 Olomouc, Czech Republic*

(Received 25 March 2014; published 9 December 2014)

Twin-beam coherence properties are analyzed in both spatial and spectral domains at high gain, including also the regime of pump depletion. We show an increase in the size of the intensity autocorrelation and cross-correlation areas at increasing pump power, replaced by a decrease in the pump depletion regime. This effect is interpreted as a progressive loss in the mode selection occurring at high-gain amplification. The experimental determination of the number of spatiospectral modes from the measurements of the $g^{(2)}$-intensity autocorrelation coefficient confirms this explanation.

DOI: 10.1103/PhysRevA.90.063812 PACS number(s): 42.65.Lm, 42.50.Ar, 85.60.Gz

I. INTRODUCTION

The process of parametric down-conversion (PDC) in bulk nonlinear crystals generates twin-beam states of light that are naturally multimode in both spectrum and space [1]. Many works, performed in the single-photon regime, have highlighted the correlations and coherence properties of photon pairs in either spectrum or space [2–10]. In the past ten years, also high-gain PDC, leading to a large number of photons per mode, has been the subject of several studies for its interesting properties of sub-shot-noise spatial intensity correlations [11–14] and macroscopic entanglement [15–20]. More recently, the spectral features of macroscopic twin-beam states have been investigated in the collinear interaction geometry close to frequency degeneracy [21]. Moreover, in the high-gain regime, the X-shaped coherence of the PDC output field [22] and the X-shaped spatiotemporal twin-beam near-field correlations [23–25], originating from the space-time coupling in the phase matching, have been demonstrated. The high-gain PDC process is also the focus of attention for its potential applications. For instance, high-gain PDC has been used for quantum imaging [26], ghost imaging [27], and absolute calibration of photodetectors [28,29]. The possibility to involve such bright states in interactions with material quantum objects (atoms, molecules, and quantum dots) also has been addressed. Moreover, the application of twin beams to quantum memories has been recently suggested [30].

In this paper we present the joint experimental investigation of spatial and spectral features of twin-beam states produced in the high-gain regime with non-negligible pump depletion. The coherence properties at different values of pump mean power are inferred by evaluating the intensity autocorrelation and cross-correlation areas on single-shot images of the far-field (θ,λ) specklelike pattern of the PDC radiation. The initial increase with PDC gain of the size of coherence areas gradually stops and at a certain pump power is replaced by a decrease. This behavior is due to the occurrence of a progressive pump depletion, which is evidenced by the evolution of the spatial and spectral pump beam profiles. Here we propose an explanation in terms of the varying population of Schmidt paired modes [31], by extending the description used at the single-photon level to high intensity. The number of effectively populated modes is experimentally accessed by the measurement of the $g^{(2)}$-intensity autocorrelation coefficient.

II. EXPERIMENTAL SCHEME AND MAIN RESULTS

The experimental setup used for the measurement of the PDC light structure in the angular and spectral (θ,λ) domain is shown in Fig. 1. A type-I 8-mm-long β-barium-borate (BBO) crystal (with a cut angle equal to 37°) was pumped by the third-harmonic pulses (349 nm, 4.5-ps pulse duration) of a mode-locked Nd:YLF laser (High Q Laser), regeneratively amplified at 500 Hz. The full width at half maximum (FWHM) of the pump beam, collimated by means of a telescope in front of the BBO, was ∼380 μm at the lowest pump power. Indeed, the pump mean power was changed during the experiment by a half-wave plate followed by a polarizing cube beam splitter. The crystal was tuned to have phase matching at frequency degeneracy in a slightly noncollinear configuration. The broadband PDC light was collected by a 60-mm focal length lens and focused on the plane of the vertical slit of an imaging spectrometer (Lot Oriel) having a 600-line/mm grating. The angularly dispersed far-field radiation was then recorded in single shot by a synchronized electron-multiplying CCD (EMCCD) camera (iXon Ultra 897, Andor), operated at full frame resolution (512 × 512 pixels, 16-μm pixel size). The resulting resolution of the system composed of the imaging spectrometer and the EMCCD camera was 0.2 nm in spectrum and 0.015° in angle. A typical specklelike pattern is shown in Fig. 2(a). The existence of intensity correlations between the signal and idler portions of the twin beam is well supported by the presence of symmetrical speckles around the degenerate wavelength and the collinear direction.

The evolution of the patterns at different pump mean powers P, and hence at different PDC gains, was investigated by calculating the intensity correlation coefficient between a single pixel at coordinates (i,j) and all the pixels (k,l)

*alessia.allevi@uninsubria.it

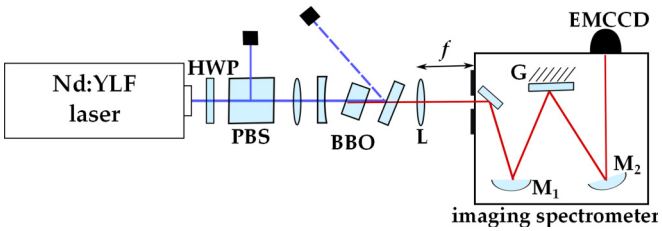

FIG. 1. (Color online) Experimental setup used for the spatiospectral measurements of the twin beam: HWP, half-wave plate; PBS, polarizing cube beam splitter; BBO, nonlinear crystal; L, lens, with 60-mm focal length; M_j, spherical mirrors; G, grating; and EMCCD, electron-multiplying camera.

contained in a single image

$$\Gamma^{(i,j)}_{k,l} = \frac{\langle I_{i,j} I_{k,l} \rangle}{\langle I_{i,j} \rangle \langle I_{k,l} \rangle}, \tag{1}$$

where $I_{m,n}$ is the intensity value of each pixel expressed in digital numbers and upon subtraction of the mean value of the noise measured with the camera in perfect dark, whereas angular brackets indicate averaging over a sequence of 1000 subsequent images. The procedure was applied to a set of pixels having the abscissa i close to frequency degeneracy and the ordinate j in the quasicollinear direction. The function $\Gamma^{(i,j)}_{k,l}$ defined in Eq. (1) is a matrix having the same size as the original images and containing both the intensity autocorrelation and the cross-correlation areas [see Fig. 2(b)]. The horizontal section of these correlation areas is related to the spectrum, whereas the vertical section gives information about the angular dispersion. In Fig. 3 we show the behaviors of the spectral [Fig. 3(a)] and spatial [Fig. 3(b)], i.e. in angular domain, widths, FWHM, of the intensity autocorrelation and cross-correlation areas, as functions of the input pump mean

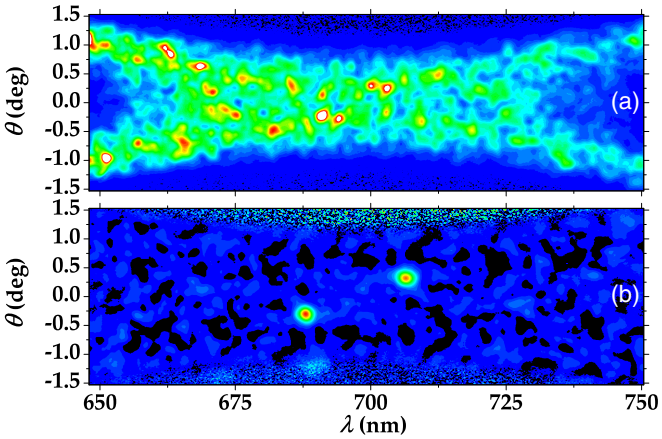

FIG. 2. (Color online) (a) Single-shot image recorded by the EMCCD camera, in which the typical specklelike pattern of PDC in the spatiospectral domain is clearly evident. (b) Typical example of the intensity correlation coefficient $\Gamma^{(i,j)}_{k,l}$, in which the intensity autocorrelation and cross-correlation areas are clearly evident. In this particular case, as the pixel at coordinates (i,j) was chosen on the left-hand side, the intensity autocorrelation area is on the same side, whereas the cross-correlation area is on the right-hand side of the image.

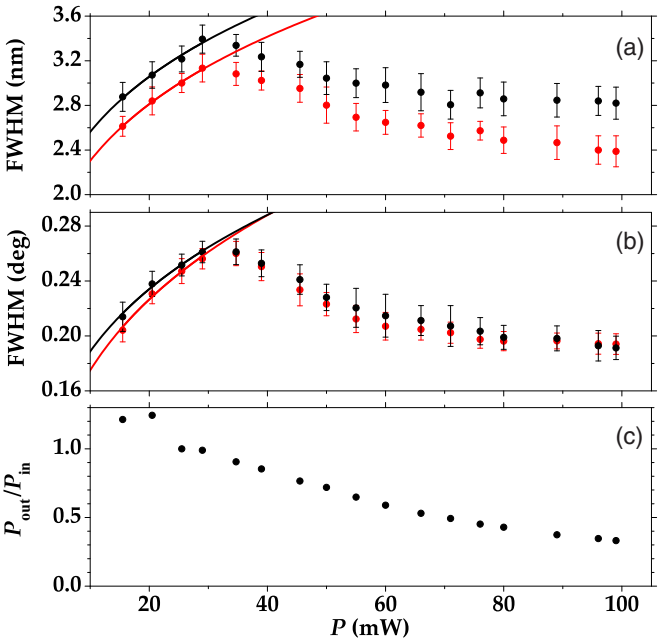

FIG. 3. (Color online) Evolutions of the (a) spectral and (b) spatial FWHM size of the intensity autocorrelation (red circles) and cross-correlation (black circles) areas measured from the (θ,λ) spectra of the twin beam as functions of the pump mean power. A fourth-root function, as expected from the theory of the PDC structure under the assumption of an undepleted pump beam, is used to fit the first part of each data set. (c) Ratio $P_{\rm out}/P_{\rm in}$ of the pump power measured at the exit of the crystal to the pump power measured at the entrance, normalized to the power value before depletion, as a function of the pump mean power.

power. In both panels we can observe an initial growth that reaches the maximum at a pump power of about 30 mW and then decreases. As shown in the figure, only the first part of the data is well described by a fourth-root function of pump power, as predicted by the theory of coherence areas under the assumption of an undepleted pump beam [13,18,27]. The second part of our experimental results (including the peak and the decrease in the FWHM) clearly indicates that the assumption of an undepleted pump beam does not hold anymore. In such a situation, also the pump beam evolves nontrivially and the corresponding equations of motion for three-mode interaction can be solved only numerically. Indeed, the behavior shown in Fig. 3 can be qualitatively reproduced by the numerical simulations of the PDC process, which will be presented in the next section.

III. FURTHER CHARACTERIZATION AND COMPARISON WITH THEORY

The numerical modeling of the experiment is fully 3D+1, i.e., it includes time and the two spatial coordinates in the plane transverse to the mean propagation direction of light z. It is formulated in terms of two coupled propagation equations along the crystal for the pump and signal field operators a_0 and a_1, respectively, in the Fourier spatiotemporal domain $(\vec{q},\Omega)$, where $\vec{q} = (q_x, q_y)$ is the transverse component of the wave vector and Ω is the frequency shift from the carrier frequencies

ω_0 and $\omega_1 = \omega_0/2$ [32,33]:

$$\frac{\partial}{\partial z}a_1(\vec{q},\Omega,z) = \sigma \int \frac{d\vec{q}\,'d\Omega'}{(2\pi)^{3/2}}[a_0(\vec{q}+\vec{q}\,',\Omega+\Omega',z) \times a_1^{\dagger}(\vec{q}\,',\Omega',z)e^{-i\Delta(\vec{q},\Omega;\vec{q}\,',\Omega')z}], \quad (2a)$$

$$\frac{\partial}{\partial z}a_0(\vec{q},\Omega,z) = -\sigma \int \frac{d\vec{q}\,'d\Omega'}{(2\pi)^{3/2}}[a_1(\vec{q}-\vec{q}\,',\Omega-\Omega',z) \times a_1(\vec{q}\,',\Omega',z)e^{i\Delta(\vec{q}',\Omega';\vec{q}-\vec{q}',\Omega-\Omega')z}]. \quad (2b)$$

The coupling constant σ in Eqs. (2) is linearly proportional to the $\chi^{(2)}$ coefficient of the nonlinear medium and the function Δ accounts for the phase mismatch between the three interacting modes:

$$\Delta(\vec{q},\Omega;\vec{q}\,',\Omega') = k_{1z}(\vec{q},\Omega) + k_{1z}(\vec{q}\,',\Omega') - k_{0z}(\vec{q}+\vec{q}\,',\Omega+\Omega'), \quad (3)$$

$k_{jz}(\vec{q},\Omega) = \sqrt{k_j(\vec{q},\Omega)^2 - q^2}$ $(j = 0,1)$ being the longitudinal components of the wave vectors $\vec{k}_j(\vec{q},\Omega)$. These equations are simulated in the framework of the Wigner representation, where field operators are replaced by c-number fields. In this context, the PDC field at the crystal entrance face, initially in the vacuum state, is simulated with Gaussian white noise, while the injected pump field is a high-intensity coherent pulse. Although the pump pulses of the experiment are not transform limited, for practical reasons we choose to model them by a Gaussian profile, with a transverse FWHM size of 250 μm and a pulse duration of 400 fs, such that the spatial and temporal bandwidths are roughly equal to the experimental ones. Clearly, when pump depletion is not negligible, the initial pump field profile undergoes significant modifications during its evolution. The propagation equations (2) are solved through a pseudospectral (split-step) integration method, where the phase-matching function (3) is calculated by using the complete Sellmeier dispersion relations for the BBO crystal found in [34] (more details on the simulation method can be found in [18]).

The results of these numerical simulations for the coherence areas are displayed in Fig. 4 and should be compared with the experimental data in Fig. 3. We see that the behavior found in the experiment is qualitatively well reproduced by the numerical simulations. We notice that the slight discrepancy between the absolute values of the experimental FWHMs and those obtained from simulations is mainly due to the uncertainty in the correct positioning of the EMCCD camera in the imaging exit plane of the spectrometer. In Figs. 3(c) and 4(c) we also show the ratio of the pump power at the exit of the crystal to the pump power at the entrance, normalized to the power value before depletion, for experimental data and simulations, respectively. The decrease of this ratio beyond a given value of pump power is a clear indication of the occurrence of pump depletion in correspondence to a narrowing of the coherence areas.

A further confirmation of the occurrence of pump depletion is given by the evolution of the spectral and spatial pump-beam profiles shown in Figs. 5 and 6 for experimental data and simulations, respectively. From the experimental point of view, we obtained the spectral profile of the pump by producing a magnified image of the near field of the pump on the

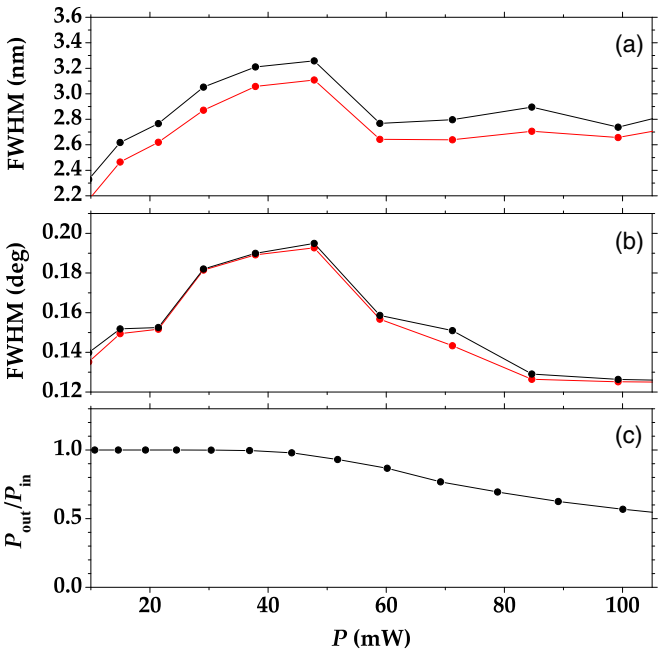

FIG. 4. (Color online) Simulations of the evolution of the (a) spectral and (b) spatial FWHM size of the intensity autocorrelation (line with red circles) and cross-correlation (line with black circles) areas of the twin beam as functions of the pump mean power. (c) Simulation of the ratio P_{out}/P_{in} of the pump power at the exit of the crystal to the pump power at the entrance, normalized to the power value before depletion, as a function of the pump mean power.

slit of the spectrometer (in this case we employed a grating characterized by 2400 lines/mm) and using a CCD camera (DCU223M, Thorlabs, 1024 × 768 pixels, 4.65-μm pixel size) to collect the light at the output. Figure 5(a) displays different sections, normalized at their peaks, corresponding to different pump mean power values. First of all, we observe that the spectrum of the pump turns out to be roughly ∼1 nm wide, thus testifying that the pump beam is non-transform-limited and also justifying the choice of a 400-fs pulse duration in the simulations. Second, we note that both the dips in the sections of Fig. 5(a) and the progressive appearance of a central hole in the contour plots shown in Figs. 5(b)–5(d) are a clear signature of pump depletion. The sections of the spatial profiles presented in Fig. 5(e) and normalized at their area were obtained by taking 1:1 images of the pump beam at the output of the crystal with the same DCU223M camera at different values of the power. Also in this case a clear dip occurs. It becomes broader and deeper as the pump mean power increases. Its generation is initially slightly lateral with respect to the center because of the pump beam walkoff inside the crystal [see Figs. 5(f)–5(h)].

The depletion of the pump is also responsible for the evolution of the total number of photons generated in each realization of the PDC process. In Fig. 7 we plot the mean number of photons detected in an area close to frequency degeneracy and in the quasicollinear interaction geometry as a function of the square root of the pump peak power per pulse. To obtain this result, we have taken into account the calibration of the camera sensitivity (5.4 electrons per digital

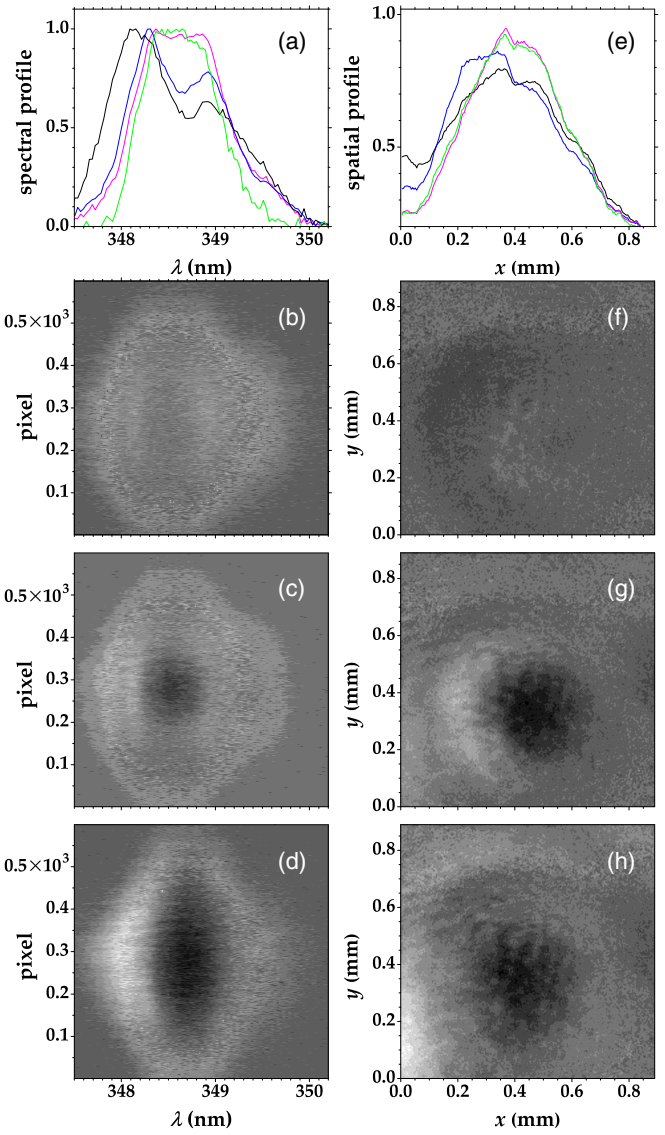

FIG. 5. (Color online) Spectral and spatial pump beam profiles for different values of the pump mean power: (a) sections of the spectral profile at different pump powers (green, 15 mW; magenta, 35 mW; blue, 55 mW; and black, 99 mW), (b)–(d) maps of the spectral distributions upon subtraction of the distribution of the least intense measurement [(b) 35 mW, (c) 55 mW, and (d) 99 mW], (e) sections of the spatial profile at different pump powers (green, 15 mW; magenta, 35 mW; blue, 55 mW; and black, 99 mW), and (f)–(h) maps of the spatial distributions upon subtraction of the distribution of the least intense measurement.

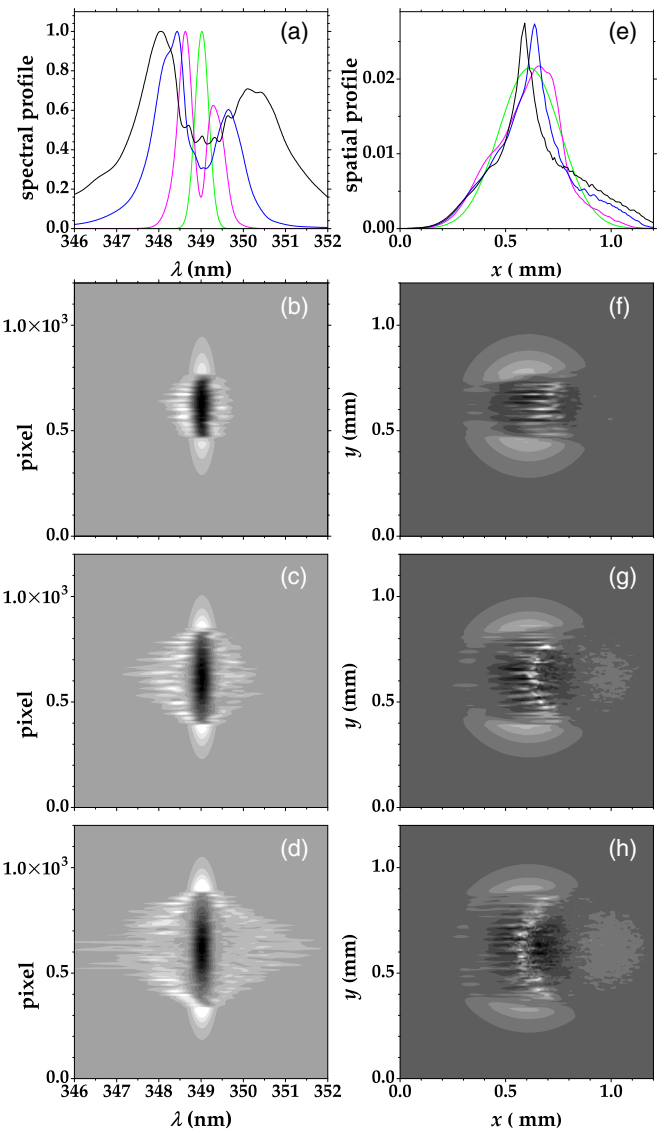

FIG. 6. (Color online) Simulation of the spectral and spatial pump beam profiles for different values of the pump mean power: (a) sections of the spectral profile at different pump powers (green, 12 mW; magenta, 30 mW; blue, 55 mW; and black, 100 mW), (b)–(d) maps of the spectral distributions upon subtraction of the distribution at the lowest power [(b) 30 mW, (c) 55 mW, and (d) 100 mW], (e) sections of the spatial profile at different pump powers (green, 12 mW; magenta, 30 mW; blue, 55 mW; and black, 100 mW), and (f)–(h) maps of the spatial distributions upon subtraction of the distribution at the lowest power.

number), its detection efficiency ($\sim 90\%$ at 698 nm), and all the optical losses. The mean number of photons shown in Fig. 7 starts increasing exponentially, as expected for high-gain PDC under the hypothesis of an undepleted pump beam. This initial behavior is emphasized in the inset of the same figure, where the experimental data corresponding to the lowest pump power values are presented together with the fitting curve function $y = A\sinh^2(Bx)$. The fitted values of A and B have been used to calculate the red curve shown in the main figure, which represents the expected gain behavior in the absence of pump depletion. In this condition, the gain of the process would vary from 5.3 up to 13.4, but the occurrence of a progressive depletion process prevents the exponential growth.

As recently demonstrated in [35], there is a correspondence between the growth of the total number of generated photons in PDC radiation and the energy lost by the pump beam in the nonlinear interaction, calculated as the difference between the number of photons expected in the pump beam in the absence of depletion and the measured mean number of pump photons. This confirms the energy-conservation law in the PDC process.

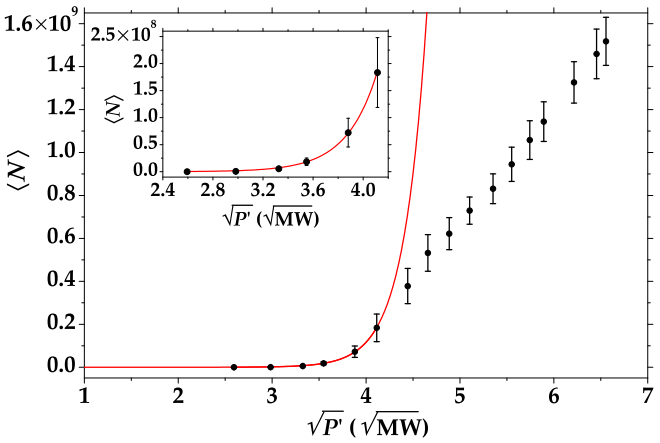

FIG. 7. (Color online) Evolution of the number of photons generated by PDC as a function of the square root of the pump peak power P' per pulse. The theoretical curve (red line) holding under the assumption of an undepleted pump beam is also shown. The inset shows the first part of the data shown in the main figure (black circles) together with the fitting curve predicted by the theory (red line).

IV. DISCUSSION AND INTERPRETATION

In order to explain the qualitative change in the evolution of the mean number of photons, as well as of the size of intensity autocorrelation and cross-correlation areas, due to pump depletion, in the following we give a consistent interpretation in terms of the modes that describe the radiation field. When the PDC process occurs at gain values leading to depletion, also the pump beam evolves in the nonlinear interaction and the dynamics of the system becomes more complex. In particular, there is a dependence of the number of effectively populated signal and idler radiation modes on the pump power. As the pump power increases, the PDC gain profile becomes narrower and narrower and thus the signal and idler fields are dominantly emitted into a smaller and smaller number of modes that gain energy to the detriment of the others [36,37]. For sufficiently high values of the pump power, the process of mode selection reverts as the pump profile undergoes depletion. For this reason, the gain of the high-population low-order modes is on the one side reduced, whereas the gain of low-population higher-order modes is on the other side supported. Such a behavior explains the narrowing of the intensity autocorrelation and cross-correlation areas shown in Fig. 3. The description in terms of populated radiation modes also explains the slight discrepancy between the autocorrelation and cross-correlation intensity functions plotted in Fig. 3. In fact, the cross-correlation function reflects the mutual coherence between the signal and idler and originates in the pairwise PDC emission, whereas the autocorrelation function expresses the internal coherence due to the presence of three evolving fields. As such, it is more sensitive to losses in the modes selection [38].

To give a quantitative evaluation of such modes, we first consider the theory of PDC at the single-photon level that expresses a bipartite state of biphotons as a sum of factorized terms [31,39] $|\Psi_{12}\rangle = \sum_k \lambda_k |u_k\rangle|v_k\rangle$. Here $|u_k\rangle$ and $|v_k\rangle$ represent the eigenvectors of an orthonormal dual basis (the Schmidt modes). The eigenvalues λ_k of the decomposition give the probabilities p_k of detecting a photon in the kth mode $p_k = \lambda_k^2$.

For more intense twin beams, probabilities p_k are derived from mean intensities $\langle I_k\rangle$ of, e.g., the signal field along the formula $p_k = \langle I_k\rangle/\langle I\rangle$, in which $I = \sum_k I_k$ is the overall intensity. An effective number of populated spatiospectral modes K is then determined as [40,41]

$$K = \frac{1}{\sum_k p_k^2}. \tag{4}$$

Assuming thermal statistics of individual modes k generated at high-gain PDC (even with pump depletion) [35], the relation $\langle I_k^2\rangle = 2\langle I_k\rangle^2$ holds [42]. Then Eq. (4) can be rewritten in the form

$$K = \frac{\left(\sum_k \langle I_k\rangle\right)^2}{\sum_k \langle I_k\rangle^2} = \frac{\left(\sum_k \langle I_k\rangle\right)^2}{\sum_k \left(\langle I_k^2\rangle - \langle I_k\rangle^2\right)}. \tag{5}$$

On the other hand, the intensity autocorrelation coefficient defined as $g^{(2)} = \langle I^2\rangle/\langle I\rangle^2$ [42] is expressed as

$$g^{(2)} = 1 + \frac{\sum_k \left(\langle I_k^2\rangle - \langle I_k\rangle^2\right)}{\left(\sum_k \langle I_k\rangle\right)^2}. \tag{6}$$

A comparison of Eqs. (5) and (6) finally provides the formula

$$g^{(2)} = 1 + 1/K \tag{7}$$

used for the determination of the number K of modes. We notice that in the high-gain regime there is also a relevant quantum correlation between the signal and idler photon numbers inside independent spatiospectral modes. For this reason, the evaluation of the number of spatiospectral modes is not sufficient to determine the quantum Schmidt number quantifying the entanglement of the state and further considerations are needed [43].

With the goal of investigating how the variation of the coherence area is affected by a variation in the number of effectively populated modes, we therefore evaluated the peak of the intensity correlation as a function of the pump power. More precisely, we evaluated $g^{(2)}$ as the autocorrelation coefficient in Eq. (1) over a single pixel $\Gamma_{i,j}^{(i,j)}$ so that we can exploit the minimum resolution [44] of our detection system, namely, 0.2 nm in spectrum and 0.015° in angle. The procedure was applied to a set of pixels close to the frequency degeneracy and in the nearly collinear direction. In Fig. 8(a) we present the dependence of the maximum values of the intensity autocorrelation coefficient on increasing values of the pump mean power. We note that $g^{(2)}$ is evaluated in both the signal (closed circles) and idler arms (open circles). As already observed in Fig. 3 for the size of the intensity autocorrelation and cross-correlation areas, the plot exhibits a peak for the pump power of 30 mW, which lies at the beginning of the pump depletion regime. By using Eq. (7), we estimate the number K of modes, as shown in Fig. 8(b). The comparison of Figs. 3 and 8(b) confirms the complementary behavior of sizes of the intensity autocorrelation and cross-correlation areas and numbers of modes. Also a close similarity between the number K of modes assigned to the signal and to the idler

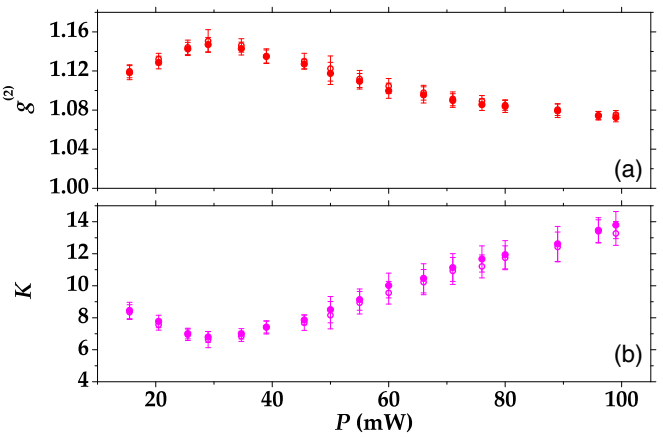

FIG. 8. (Color online) (a) Intensity autocorrelation coefficient (red circles) dependent on the pump mean power and (b) number K of spatiospectral modes determined from the $g^{(2)}$-intensity autocorrelation coefficient. In both panels the data shown as closed (open) circles characterize the signal (idler) arm.

arms is noticeable. At low pump powers, where no filters were used to attenuate the light of twin beams, the numbers K are nearly identical. We note that the dual basis revealed in the Schmidt decomposition [45,46] can successfully be replaced for more intense fields by the input-output eigenmodes of the Bloch-Messiah reduction of the signal-idler unitary evolution operators [41].

V. CONCLUSION

We have presented an experimental investigation of the spatiospectral properties of PDC in the high-gain regime including pump depletion. The evolution of the pump is responsible for the qualitative change in the size of intensity autocorrelation and cross-correlation areas for increasing pump power. While the intensity autocorrelation and cross-correlation areas gradually broaden for lower pump power values, they undergo narrowing at increasing high pump powers. We explain this behavior by the change in the number of effectively populated paired modes, whose complementary behavior compared to the sizes of the intensity autocorrelation and cross-correlation areas has been experimentally confirmed. These results provide clear evidence that the properties of nonlinear processes at high intensities reflect a complex internal mode structure, which is, in contrast, well known for fields with intensities at the single-photon level. Our findings are by no means restricted to parametric down-conversion, as they can be generalized to other nonlinear processes, such as Raman or Brillouin processes.

ACKNOWLEDGMENTS

This work was supported by MIUR under Grant No. FIRB LiCHIS-RBFR10YQ3H. J.P. and O.H. acknowledge Project No. P205/12/0382 of GA ČR and Projects No. CZ.1.05/2.1.00/03.0058 and No. CZ.1.07/2.3.00/20.0058 of MŠMT ČR. O.J. thanks Paolo Di Trapani for fruitful discussions.

[1] A. Allevi, S. Olivares, and M. Bondani, Phys. Rev. A **85**, 063835 (2012).
[2] M. Hamar, J. Peřina Jr., O. Haderka, and V. Michálek, Phys. Rev. A **81**, 043827 (2010).
[3] J.-L. Blanchet, F. Devaux, L. Furfaro, and E. Lantz, Phys. Rev. Lett. **101**, 233604 (2008).
[4] P.-A. Moreau, J. Mougin-Sisini, F. Devaux, and E. Lantz, Phys. Rev. A **86**, 010101(R) (2012).
[5] B. Dayan, A. Peer, A. A. Friesem, and Y. Silberberg, Phys. Rev. Lett. **94**, 043602 (2005).
[6] A. Peer, B. Dayan, A. A. Friesem, and Y. Silberberg, Phys. Rev. Lett. **94**, 073601 (2005).
[7] K. A. O'Donnell and A. B. U'Ren, Phys. Rev. Lett. **103**, 123602 (2009).
[8] S. Sensarn, G. Y. Yin, and S. E. Harris, Phys. Rev. Lett. **104**, 253602 (2010).
[9] O. Haderka, J. Peřina Jr., M. Hamar, and J. Peřina, Phys. Rev. A **71**, 033815 (2005).
[10] J. Peřina Jr., M. Hamar, V. Michálek, and O. Haderka, Phys. Rev. A **85**, 023816 (2012).
[11] O. Jedrkiewicz, Y.-K. Jiang, E. Brambilla, A. Gatti, M. Bache, L. A. Lugiato, and P. Di Trapani, Phys. Rev. Lett. **93**, 243601 (2004).
[12] M. Bondani, A. Allevi, G. Zambra, M. G. A. Paris, and A. Andreoni, Phys. Rev. A **76**, 013833 (2007).
[13] G. Brida, L. Caspani, A. Gatti, M. Genovese, A. Meda, and I. Ruo Berchera, Phys. Rev. Lett. **102**, 213602 (2009).
[14] I. N. Agafonov, M. V. Chekhova, and G. Leuchs, Phys. Rev. A **82**, 011801(R) (2010).
[15] W. J. Munro and M. D. Reid, Phys. Rev. A **47**, 4412 (1993).
[16] C. Simon and D. Bouwmeester, Phys. Rev. Lett. **91**, 053601 (2003).
[17] A. Gatti, R. Zambrini, M. San Miguel, and L. A. Lugiato, Phys. Rev. A **68**, 053807 (2003).
[18] E. Brambilla, A. Gatti, M. Bache, and L. A. Lugiato, Phys. Rev. A **69**, 023802 (2004).
[19] T. Iskhakov, M. V. Chekhova, and G. Leuchs, Phys. Rev. Lett. **102**, 183602 (2009).
[20] C. Vitelli, N. Spagnolo, L. Toffoli, F. Sciarrino, and F. De Martini, Phys. Rev. A **81**, 032123 (2010).
[21] K. Yu. Spasibko, T. Sh. Iskhakov, and M. V. Chekhova, Opt. Express **20**, 7507 (2012).
[22] O. Jedrkiewicz, A. Picozzi, M. Clerici, D. Faccio, and P. Di Trapani, Phys. Rev. Lett. **97**, 243903 (2006).
[23] A. Gatti, E. Brambilla, L. Caspani, O. Jedrkiewicz, and L. A. Lugiato, Phys. Rev. Lett. **102**, 223601 (2009).
[24] O. Jedrkiewicz, J.-L. Blanchet, E. Brambilla, P. Di Trapani, and A. Gatti, Phys. Rev. Lett. **108**, 253904 (2012).
[25] O. Jedrkiewicz, A. Gatti, E. Brambilla, and P. Di Trapani, Phys. Rev. Lett. **109**, 243901 (2012).
[26] G. Brida, M. Genovese, and I. Ruo Berchera, Nat. Photon. **4**, 227 (2010).
[27] M. Bondani, A. Allevi, and A. Andreoni, Eur. Phys. J. Spec. Top. **203**, 151 (2012).

[28] G. Brida, I. P. Degiovanni, M. Genovese, M. L. Rastello, and I. Ruo-Berchera, Opt. Express **18**, 20572 (2010).
[29] I. N. Agafonov, M. V. Chekhova, T. S. Iskhakov, A. N. Penin, G. O. Rytikov, and O. A. Shcherbina, Opt. Lett. **36**, 1329 (2011).
[30] L. V. Gerasimov, I. M. Sokolov, D. V. Kupriyanov, and M. D. Havey, J. Phys. B **45**, 124012 (2012).
[31] C. K. Law and J. H. Eberly, Phys. Rev. Lett. **92**, 127903 (2004).
[32] E. Brambilla, O. Jedrkiewicz, L. A. Lugiato, and A. Gatti, Phys. Rev. A **85**, 063834 (2012).
[33] E. Brambilla, O. Jedrkiewicz, P. Di Trapani, and A. Gatti, J. Opt. Soc. Am. B **31**, 1383 (2014).
[34] N. Boeuf, D. Branning, I. Chaperot, E. Dauler, S. Guerin, G. Jaeger, A. Muller, and A. Migdall, Opt. Eng. **39**, 1016 (2000).
[35] A. Allevi and M. Bondani, J. Opt. Soc. Am. B **31**, B14 (2014).
[36] W. Wasilewski, A. I. Lvovsky, K. Banaszek, and C. Radzewicz, Phys. Rev. A **73**, 063819 (2006).
[37] A. M. Perez, T. Sh. Iskhakov, P. Sharapova, S. Lemieux, O. V. Tikhonova, M. V. Chekhova, and G. Leuchs, Opt. Lett. **39**, 2403 (2014).
[38] R. Machulka, O. Haderka, J. Peřina Jr., M. Lamperti, A. Allevi, and M. Bondani, Opt. Express **22**, 13374 (2014).
[39] A. Christ, K. Laiho, A. Eckstein, K. N. Cassemiro, and C. Silberhorn, New J. Phys. **13**, 033027 (2011).
[40] A. Gatti, T. Corti, E. Brambilla, and D. B. Horoshko, Phys. Rev. A **86**, 053803 (2012).
[41] J. Peřina Jr., Phys. Rev. A **87**, 013833 (2013).
[42] J. Peřina, *Quantum Statistics of Linear and Nonlinear Optical Phenomena* (Kluwer, Dordrecht, 1991).
[43] A. Gatti "The Schmidt number of entanglement of high gain twin beams" (unpublished).
[44] K. Laiho, A. Christ, K. N. Cassemiro, and C. Silberhorn, Opt. Lett. **36**, 1476 (2011).
[45] S. S. Straupe, D. P. Ivanov, A. A. Kalinkin, I. B. Bobrov, and S. P. Kulik, Phys. Rev. A **83**, 060302(R) (2011).
[46] A. Avella, M. Gramegna, A. Shurupov, G. Brida, M. Chekhova, and M. Genovese, Phys. Rev. A **89**, 023808 (2014).